ELSEVIER

Journal of Nuclear Materials 266–269 (1999) 526–531

journal of nuclear materials

Numerical analysis of thermoelectric instability in tokamak divertor

N. Hayashi [a,*], T. Takizuka [b], A. Hatayama [a], M. Ogasawara [a]

[a] *Faculty of Science and Technology, Department of Applied Physics and Physico-Informatics 3-14-1 Hiyoshi, Kouhoku-ku, Keio University, Yokohama 223-0061, Japan*

[b] *Naka Fusion Research Establishment, Japan Atomic Energy Research Institute, Ibaraki 311-0193, Japan*

Abstract

The thermoelectric instability in tokamak divertor has been studied numerically by using a five-point model. When the divertor plasma temperature T_{div} decreases below a critical temperature, this instability arises in a symmetric equilibrium of scrape-off layer (SOL) and divertor plasmas, and stable asymmetric equilibria are found. The SOL current causes spontaneously the divertor asymmetry at the onset of the thermoelectric instability. In an asymmetric equilibrium, the SOL current flows from the higher-T_{div} side to the lower-T_{div} side. The heat flux flowing into the divertor plate of the higher-T_{div} side becomes larger than that of the lower-T_{div} side. The heat flux asymmetry is larger for cases of high recycling and low heating power.

Keywords: SOL current; Divertor asymmetry; Divertor modeling

1. Introduction

The parallel current in the SOL plasma has been experimentally observed in several tokamaks [1,2], and is considered as one of the causes of the divertor asymmetry. The critical point for the onset of the asymmetry taking account of the SOL current has been studied analytically and numerically by Staebler [3]. He showed that the SOL current spontaneously generates the divertor asymmetry at the critical point. On the other hand, the instability caused by the SOL current has been pointed out qualitatively by LaBombard [1]. The mechanism of the instability is schematically shown in Fig. 1. The electron temperature asymmetry, $T_{sA} > T_{sB}$ in Fig. 1, causes the sheath potential difference between the both ends of the magnetic field line. This thermoelectric effect generates the SOL current j flowing from the high-temperature side A to the low-temperature side B. The SOL current j drives an asymmetric heat flux q_j in the opposite direction of the current, which carries the electron energy from the low-temperature side B to the high-temperature side A. This heat flux asymmetry, in turn, increases the electron temperature asymmetry. This instability is called ''thermoelectric instability''.

In this paper, we investigate numerically the divertor asymmetry from the viewpoint of the thermoelectric instability by using a five-point model [4] for SOL and divertor plasmas. Symmetric and asymmetric equilibria of the SOL and divertor plasmas are quantitatively obtained and the stability of the equilibria is analyzed.

2. Five-point model for SOL and divertor plasmas

We analyze the thermoelectric instability by using a five-point model. Fig. 1 also shows a geometry of the model. The detailed model is described in Ref. [4].

2.1. Fluid equations

The model is based on fluid equations, i.e., particle, momentum, energy, generalized Ohm's law, and current equations. We investigate attached divertor plasmas in the present study, and the momentum equation does not

* Corresponding author. Tel.: +81 45 563 1151/3516; fax: +81 45 563 0322; e-mail: hayashi@ppl.appi.keio.ac.jp.

0022-3115/99/$ – see front matter
PII: S0022-3115(98)00832-0

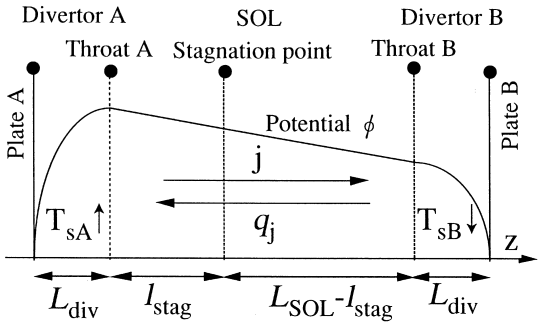

Fig. 1. Electrostatic potential in asymmetric SOL-divertor plasma with $T_{sA} > T_{sB}$. SOL current j carrying heat flux q_j drives thermoelectric instability. Geometry for five-point model is also shown.

take account of the momentum loss. Perpendicular currents are not taken into account, for simplicity. Some of the important equations in the model as described as follows. Equations for the energy and generalized Ohm's law are given as

$$\frac{\partial}{\partial z}(q + \phi j) = W, \tag{1}$$

$$\frac{\partial \phi}{\partial z} = -\eta j + \frac{\alpha}{e}\frac{\partial T}{\partial z} + \frac{1}{en}\frac{\partial (nT)}{\partial z}\ , \tag{2}$$

where z is the length along the magnetic field and the thermal force coefficient α is given as $\alpha = 0.71$ for singly charged particles [5]. Quantities ϕ, j, and n, denote the electrostatic potential, SOL current density parallel to the magnetic field, and plasma density, respectively. We assume that the electron temperature T_e and the ion temperature T_i are the same for simplicity, $T_e = T_i = T$. The electric resistivity η is given as $\eta = \eta_x \cdot T^{-3/2}$. The parallel heat flux of the sum of the ion's and electron's, q, includes both conductive and convective fluxes,

$$q = -\kappa_{e\|}\frac{\partial T}{\partial z} - \left(\frac{5}{2} + \alpha\right)\frac{j}{e}T + 5T\Gamma, \tag{3}$$

where Γ denotes a parallel ion particle flux. The electron heat conductivity parallel to the magnetic field $\kappa_{e\|}$ is given as $\kappa_{e\|} = \kappa_* T^{5/2}$. The current drives an heat transport in the opposite direction of the current as given by the second term in RHS of Eq. (3).

The energy source term W in RHS of Eq. (1) is defined in each region as explained as follows. In the SOL region, the source term W_{SOL} takes account of the radial diffusion of the energy into the SOL from the core plasma. In the divertor region, the source term W_{div} takes account of the energy loss due to the ionization of neutrals and the impurity radiation, and is assumed to be given by $W_{div} = -k\Delta E S_N$ where ΔE and S_N denote the ionization energy per an ionization event ($\Delta E = 13.6$ eV) and the plasma particle source due to the ionization of neutrals, respectively. The effective enhancing factor k is chosen to be 4, which is an empirical value for JT-60U experiments [6].

Boundary conditions at the entrance in front of a divertor plate are given on the basis of the sheath theory [7] as follows. The parallel ion particle flux Γ_s and the parallel heat flux q_s are given by $\Gamma_s = n_s\sqrt{2T_s/m}$ and $q_s = \gamma_s \Gamma_s T_s$, respectively. The heat transmission coefficient γ_s and the current density j are given by

$$\gamma_s = \gamma_* - (2+\beta)\frac{j}{e\Gamma_s} - \left(1 - \frac{j}{e\Gamma_s}\right)\ln\left(1 - \frac{j}{e\Gamma_s}\right), \tag{4}$$

$$\frac{j}{e\Gamma_s} = 1 - \exp\left\{\beta - \frac{e}{T_s}(\phi_s - \phi_p)\right\}, \tag{5}$$

where the subscripts s and p correspond to the sheath entrance and the divertor plate, respectively. Values of β and γ_* for deuterium plasma are 2.8 [7] and 7.8 [6], respectively.

2.2. Extension of five-point model

In Ref. [4], the model employed an approximation that the temperature is uniform in the SOL region and T_{uA} and T_{uB} at the up-stream throat of each divertor region are the same, $T_{uA} = T_{uB} = T_0$. This approximation, however, is not always adequate for the analysis of the thermoelectric instability because the energy flux carried by the SOL current into (or out of) the divertor region, $-(5/2+\alpha)jT_u/e$, plays an important role to cause the thermoelectric instability. In this paper, we take account of the variation of the SOL temperature. The conductive parts in Eq. (3) at the throat A and B are written as

$$\kappa_{e\|}\left.\frac{\partial T}{\partial z}\right|_{uA} = -\frac{2}{7}\kappa_*\frac{T_{sA}^{7/2} - T_{uA}^{7/2}}{L_{div}} = -\frac{4}{7}\kappa_*\frac{T_{uA}^{7/2} - T_0^{7/2}}{l_T}, \tag{6}$$

$$-\kappa_{e\|}\left.\frac{\partial T}{\partial z}\right|_{uB} = -\frac{2}{7}\kappa_*\frac{T_{sB}^{7/2} - T_{uB}^{7/2}}{L_{div}} = -\frac{4}{7}\kappa_*\frac{T_{uB}^{7/2} - T_0^{7/2}}{L_{SOL} - l_T}. \tag{7}$$

The length l_T is measured from the left-side throat of the divertor region A, and corresponds to the position where the temperature has a maximum value T_0. The equation for l_T is given by integrating Eq. (1) in the SOL regions with the use of Eqs. (2) and (3),

$$l_T = \frac{L_{SOL}}{2} - \frac{q_{uB} - q_{uA} + 5T_0 j/e + \alpha(T_{uB} + T_{uA})j/e}{2(W_{SOL} + \eta_* T_0^{-3/2} j^2)}. \tag{8}$$

Note that the position denoted by l_T is different from the stagnation point denoted by l_{stag}.

We next extend the model for the stability analysis. Instead of T_{sA} and T_{sB}, we introduce new variables, $T_d \equiv (T_{sB} + T_{sA})/2$ and $\sigma \equiv (T_{sB} - T_{sA})/T_d$. The variable σ indicates the degree of the asymmetry in the divertor plasma temperature. The equilibrium is symmetric at $\sigma = 0$. Eq. (1) is modified to include a time differential term and is integrated in each SOL and divertor region. As a result, time differentiations of T_0, T_d and σ are summarized as

$$\frac{dT_0}{dt} = F_1(T_0,\ T_d,\ \sigma), \quad \frac{dT_d}{dt} = F_2(T_0,\ T_d,\ \sigma),$$
$$\frac{d\sigma}{dt} = F_3(T_0,\ T_d,\ \sigma), \tag{9}$$

The functions F_1, F_2, and F_3 are calculated when the following seven parameters are given, the radial particle diffusivity $D_\perp$, radial heat diffusivity $\chi_\perp$, total particle flow Φ_{sep}, total heat flow Q_{sep} from the core to the SOL plasma, particle flux amplification factors R_A, R_B, and potential difference between divertor plates $\phi_{pB} - \phi_{pA}$. The particle flux amplification factor R is defined by a ratio of Γ_s to the particle flux at the throat Γ_u. Thus, R characterizes the strength of the recycling in the divertor region. Steady state solutions of T_0, T_d and σ are obtained from the calculations $F_1 = F_2 = F_3 = 0$. We analyze the equilibrium and stability in the (T_d, σ) plane. At first, the SOL temperature $T_0 = T_0(T_d, \sigma)$ is solved from a equation, $F_2 = 0$. Trajectories of the other two equations, $F_1 = 0$ and $F_3 = 0$, are drawn in the (T_d, σ) plane. An intersection between these trajectories gives an equilibrium of T_d and σ. A linear stability is analyzed by using a matrix method for Eq. (9). The details of this stability analysis method will be presented elsewhere [8].

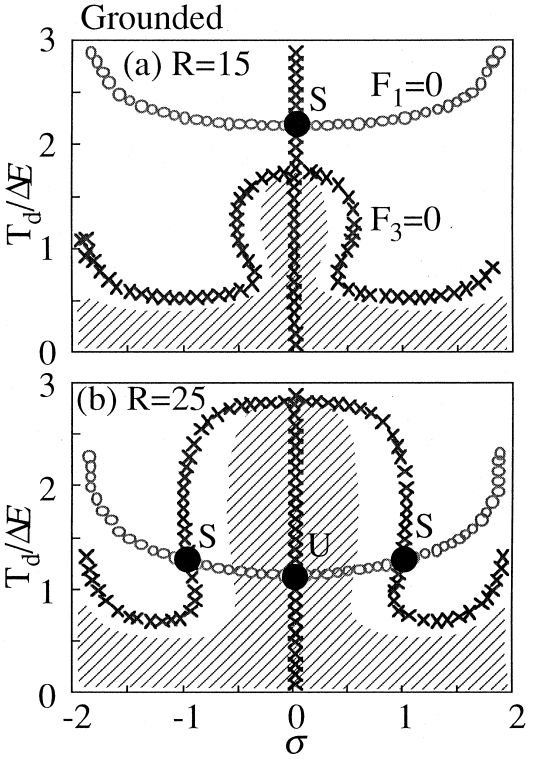

Fig. 2. Equilibrium and stability of SOL and divertor plasmas for $\Phi_{sep} = 5 \times 10^{22}$ s^{-1} and $Q_{sep} = 10$ MW in case of electrically grounded divertor plates. Flux amplification factor R is (a) $R = 15$ and (b) 25. Temperature T_d is normalized by $\Delta E = 13.6$ eV. Trajectories of $F_1 = 0$ and $F_3 = 0$ in (σ, T_d) plane are drawn with open circles and cross points. An intersection between these trajectories gives an equilibrium point. Shadow area is unstable region obtained from linear stability analysis. Closed circles S and U denote stable and unstable equilibrium points, respectively.

3. Numerical results

Numerical calculations of the equilibrium and the stability are carried out. The radial particle and thermal diffusivities are chosen as $D_\perp = 1$ m^2/s and $\chi_\perp = 2$ m^2/s, respectively [6]. The flux amplification factors R_A and R_B are the same, $R_A = R_B = R$. Geometrical parameters are $L_{SOL} = 100$ m and $L_{div} = 4$ m, which are similar to the typical parameters in JT-60U [4,9].

Fig. 2 shows equilibrium positions in (σ, T_d) plane for $\Phi_{sep} = 5 \times 10^{22}$ s^{-1} and $Q_{sep} = 10$ MW. The particle flux amplification factor R is chosen as (a) $R = 15$ and (b) 25. The plate potential difference $\phi_{pB} - \phi_{pA}$ equals zero for electrically grounded divertor plates. The two trajectories for $F_1 = 0$ and $F_3 = 0$ are drawn with open circles and cross points. An equilibrium point is plotted with a closed circle. The shadow area in Fig. 2 is the unstable region obtained from the linear stability analysis. When the recycling is low for (a) $R = 15$, a symmetric equilibrium is stable, which is drawn with a closed circle S. As the recycling increases to (b) $R = 25$, the divertor plasma temperature decreases and the symmetric equilibrium becomes unstable, which is drawn with a closed circle U.

The instability is caused by the thermoelectric instability. This is explained by comparing with the case of electrically floating divertor plates, as shown in Fig. 3. The SOL current j is fixed zero and the plate potential difference $\phi_{pB} - \phi_{pA}$ is determined self-consistently. The parameters $\Phi_{sep} = 5 \times 10^{22}$ s^{-1}, $Q_{sep} = 10$ MW and $R = 25$ are the same as those in Fig. 2(b). The thermoelectric instability disappears because the SOL current cannot flow. A stable symmetric equilibrium is obtained in Fig. 3 at the same point of (σ, T_d) as for Fig. 2(b).

When the symmetric equilibrium is unstable for the grounded divertor plates as shown in Fig. 2(b), two asymmetric equilibria are found, which have the same T_d but the opposite signs of σ with each other. These

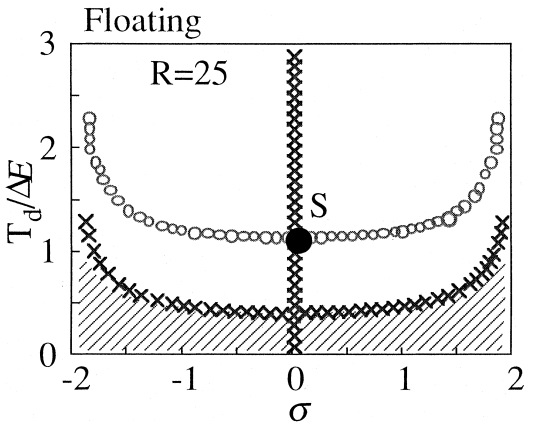

Fig. 3. Equilibrium and stability in case of electrically floating divertor plates. Parameters $\Phi_{sep} = 5 \times 10^{22}$ s^{-1}, $Q_{sep} = 10$ MW and $R = 25$ are the same as those in Fig. 2(b). Unstable point in Fig. 2(a) becomes stable.

asymmetric equilibria are stable because the following two effects stabilize the thermoelectric instability. One is the change in sheath potentials, ϕ_{sA} and ϕ_{sB}, as given by

$$\phi_{sA} - \phi_{pA} = \frac{T_{sA}}{e}\left\{\beta - \ln\left(1 + \frac{j}{e\Gamma_{sA}}\right)\right\}, \tag{10}$$

$$\phi_{sB} - \phi_{pB} = \frac{T_{sB}}{e}\left\{\beta - \ln\left(1 - \frac{j}{e\Gamma_{sB}}\right)\right\}, \tag{11}$$

which are derived from Eq. (5). For example, when T_{sA} increases and T_{sB} decreases, the first term in RHS of Eq. (10) heightens ϕ_{sA} and that of Eq. (11) lowers ϕ_{sB}. This thermoelectric effect generates the SOL current flowing from "A" to "B", i.e., $j > 0$, and causes the thermoelectric instability. On the other hand, the second term in RHS of Eq. (10) lowers ϕ_{sA}, while that of Eq. (11) heightens ϕ_{sB}. These terms decrease the thermoelectric effect with a large SOL current at the asymmetric equilibria. The other stabilizing effect is that the magnitude of the SOL current decreases with increasing the temperature asymmetry because the plasma resistivity increases in the divertor region of the lower-temperature side. These two effects stabilize the thermoelectric instability at the asymmetric equilibria.

Fig. 4 shows dependences of stable equilibrium values of (a) T_0, T_{sA}, T_{sB}, (b) j and (c) heat flux asymmetry q_{pA}/q_{pB} on the flux amplification factor R in cases of grounded and floating divertor plates. The parameters $\Phi_{sep} = 5 \times 10^{22}$ s^{-1} and $Q_{sep} = 10$ MW are the same as those in Fig. 2. The SOL current density j is normalized by $e\Gamma_d$ where $\Gamma_d \equiv \Phi_{sep}/(4\pi\theta r_m \lambda_\Gamma)$. The pitch of the magnetic field θ and the major radius r_m are $\theta = 0.06$ and $r_m = 3$ m, which are similar to the typical parameters in JT-60U [4,6,9]. The radial e-folding length λ_Γ for the particle flux is determined self-consistently in the

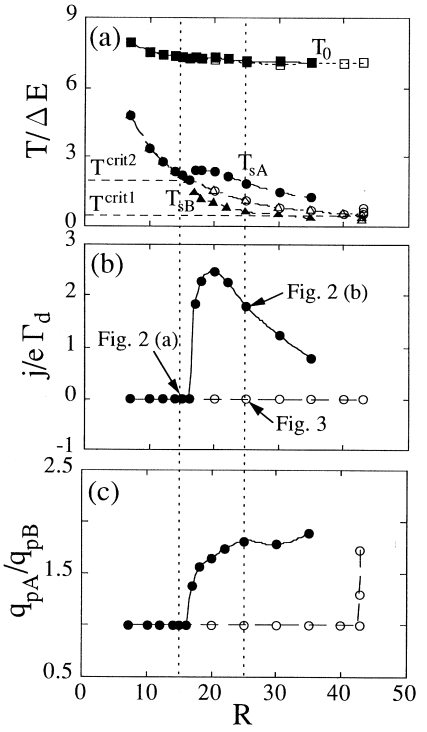

Fig. 4. Dependences of stable equilibrium values of (a) T_0, T_{sA}, T_{sB}, (b) j and (c) q_{pA}/q_{pB} on particle flux amplification factor R in cases of grounded (closed symbols) and floating (open symbols) divertor plates. Parameters $\Phi_{sep} = 5 \times 10^{22}$ s^{-1} and $Q_{sep} = 10$ MW are the same as those in Fig. 2. Temperatures T_0, T_{sA} and T_{sB} are normalized by $\Delta E = 13.6$ eV. Arrows at $R = 15$ and 25 denote the same equilibria as those in Fig. 2 (a), (b) and 3.

calculations. The value of λ_Γ changes only slightly around 4 cm in the parameter range of this paper. Thus, the value of $e\Gamma_d$ is about 90 kA/m^2. The heat fluxes flowing into the divertor plates q_{pA} and q_{pB} are defined as,

$$q_{pA} = q_{sA} - (\phi_{sA} - \phi_{pA})j, \tag{12}$$

$$q_{pB} = q_{sB} + (\phi_{sB} - \phi_{pB})j, \tag{13}$$

where the second terms denote the electric heating or cooling due to the current flowing in the potential difference between the sheath entrance and the plate. In Fig. 4, one asymmetric equilibrium with $T_{sA} \geqslant T_{sB}$ is drawn and the other asymmetric equilibrium with $T_{sA} \leqslant T_{sB}$ is obtained only by replacing the subscript A and B each other and j with $-j$. The symmetric equilibrium in Fig. 2(a) and that in Fig. 3 correspond with those at $R = 15$ and 25 in Fig. 4, respectively. The asymmetric equilibrium in Fig. 2(b) also corresponds with that at $R = 25$ in Fig. 4.

As shown in Fig. 4, the symmetric equilibrium is the same between two cases, floating and grounded divertor plates. When R increases from 7 to 43, symmetric $T_s/\Delta E$ decreases from 4.8 to 0.5 and $T_0/\Delta E$ decreases a little from 7.9 to 7.1 as shown in Fig. 4(a). In the case of floating divertor plates without the SOL current, the symmetric equilibrium becomes unstable below a critical divertor plasma temperature T^{crit1} which is due to the thermal instability of the divertor radiation as predicted by Borrass [10]. At the onset of the thermal instability, the divertor radiation spontaneously generates the divertor asymmetry as also found by Staebler [3].

In the case of grounded divertor plates with the SOL current, on the other hand, the symmetric equilibrium becomes unstable due to the thermoelectric instability at a higher temperature T^{crit2} than T^{crit1} as shown in Fig. 4(a). The divertor asymmetry is generated at the onset of the thermoelectric instability. When R increases from $R = 16$ at T^{crit2} to 35, the difference of $T_{\mathrm{sA}} - T_{\mathrm{sB}}$ increases up to 19 eV and gradually decreases. The SOL temperature T_0 of the asymmetric equilibrium is almost the same as that of the stable symmetric equilibrium for floating divertor plates.

In an asymmetric equilibrium, the SOL current j flows from higher-T_s side A to the lower-T_s side B as shown in Fig. 4(b). The SOL current j steeply increases to a certain value and decreases when R increases. This decrement of j is explained by the following two reasons. One is that the difference of $T_{\mathrm{sA}} - T_{\mathrm{sB}}$, which causes the thermoelectric potential difference, decreases when R increases from about 20 as shown in Fig. 4(a). The other is that the plasma resistivity increases with R in both divertor regions because T_{sA} and T_{sB} both decrease with increasing R as shown in Fig. 4(a).

The heat flux asymmetry $q_{\mathrm{pA}}/q_{\mathrm{pB}}$ increases and reaches to about 1.9 when R increases to 35 as shown in Fig. 4(c). The heat flux flowing into the divertor plate of the higher-T_s side A becomes larger than that of the lower-T_s side B. This heat flux asymmetry at the divertor plate is smaller than that at the sheath entrance, $q_{\mathrm{sA}}/q_{\mathrm{sB}}$, when the SOL current flows. This is because the electric heating and cooling as given by the second terms in RHS of Eqs. (12) and (13) mitigate the asymmetry $q_{\mathrm{sA}}/q_{\mathrm{sB}}$. For example, in the case of $T_{\mathrm{sA}} > T_{\mathrm{sB}}$ and $j > 0$, the electric cooling occurs in the sheath of the divertor A while the heating occurs in that of the divertor B. When the magnitude of j has its maximum value at $R = 20$, the asymmetry $q_{\mathrm{sA}}/q_{\mathrm{sB}}$ has its maximum value which is about 20% larger than $q_{\mathrm{pA}}/q_{\mathrm{pB}}$.

Fig. 5 shows dependences of stable equilibrium values of (a) T_0, T_{sA}, T_{sB}, (b) j and (c) $q_{\mathrm{pA}}/q_{\mathrm{pB}}$ on the total heat flow Q_{sep}. The parameters Φ_{sep} and R are $\Phi_{\mathrm{sep}} = 5 \times 10^{22}$ s^{-1} and $R = 15$. The symmetric equilibrium in Fig. 2(a) corresponds with that at $Q_{\mathrm{sep}} = 10$ MW in Fig. 5. The normalized SOL temperature $T_0/\Delta E$ is almost proportional to Q_{sep} and increases from 5.7 to 8.5

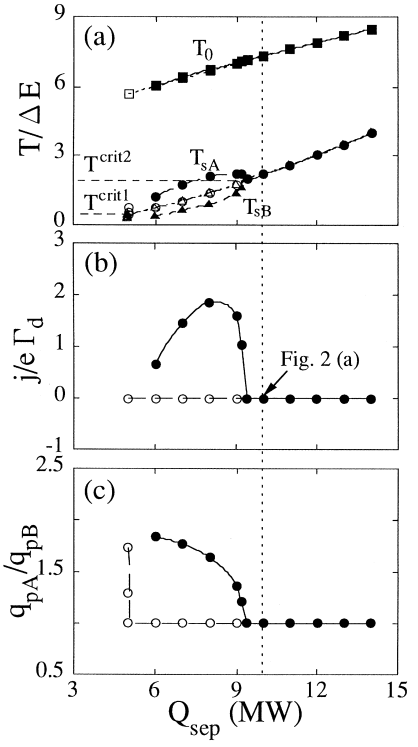

Fig. 5. Dependences of stable equilibrium values of (a) T_0, T_{sA}, T_{sB}, (b) j and (c) $q_{\mathrm{pA}}/q_{\mathrm{pB}}$ on total energy flow Q_{sep} in cases of grounded (closed symbols) and floating (open symbols) divertor plates. Parameters Φ_{sep} and R are chosen to be $\Phi_{\mathrm{sep}} = 5.0 \times 10^{22}$ s^{-1} and $R = 15$. Arrow at $R = 10$ denotes the same equilibrium as that in Fig. 2(a).

when Q_{sep} increases from 5 to 14 MW. In the case of floating divertor plates, the symmetric equilibrium value of T_s decreases to T^{crit1} when Q_{sep} decreases to 5 MW. The asymmetric equilibria are generated at T^{crit1}. In the case of grounded divertor plates, the divertor asymmetry arises at T^{crit2} higher than T^{crit1}. When Q_{sep} decreases from 9.4 MW at T^{crit2}, the difference of $T_{\mathrm{sA}} - T_{\mathrm{sB}}$ increases to 16 eV and gradually decreases until T_{sB} decreases below 5 eV. As shown in Fig. 5(b), the SOL current j flowing from "A" to "B" increases to a certain value and decreases with decreasing Q_{sep}. This decrement of j is due to the decrement of the difference of $T_{\mathrm{sA}} - T_{\mathrm{sB}}$ and the increment of the plasma resistivity in SOL and both divertor regions. The asymmetry $q_{\mathrm{pA}}/q_{\mathrm{pB}}$ increases to about 1.8 when Q_{sep} decreases to 6 MW as shown in Fig. 5(c).

4. Summary and discussion

The thermoelectric instability in tokamak divertor has been studied numerically by using a five-point model

for SOL and divertor plasmas. When the divertor plasma temperature T_{div} is high, a symmetric equilibrium of the SOL and divertor plasmas is stable. As the divertor plasma temperature decreases below a critical temperature, the symmetric equilibrium becomes unstable because of the thermoelectric instability. When the symmetric equilibrium is unstable, stable asymmetric equilibria are found. The SOL current causes spontaneously the divertor asymmetry at the onset of the thermoelectric instability. In an asymmetric equilibrium, the SOL current flows from the higher-T_{div} side to the lower-T_{div} side. The heat flux flowing into the divertor plate of the higher-T_{div} side becomes larger than that of the lower-T_{div} side. The dependence of the asymmetry on the recycling and the heating power are investigated quantitatively. The heat flux asymmetry is large for cases of high recycling and low heating power.

The thermoelectric instability due to the SOL current can be one of the key factors to generate the divertor asymmetry in the case of electrically grounded divertor plates. The detailed analysis of the onset condition for the thermoelectric instability, e.g., k dependence of T^{crit2}, will be presented elsewhere [8]. The thermoelectric instability and the resultant asymmetry under detached plasma conditions will be investigated in the future.

Acknowledgements

We wish to thank Drs N. Asakura and K. Shimizu for their discussion about results of divertor experiment in JT-60U. One of the authors (N.H.) is grateful to Drs H. Shirai, T. Hirayama, M. Kikuchi, M. Shimada and M. Azumi for their continuous supports and encouragements during his stay in JAERI as a fellow of advanced science.

References

[1] B. LaBombard et al., J. Nucl. Mater. 241–243 (1997) 149.
[2] A. Kumagai, et al., Plasma Phys. Control. Fusion 39 (1997) 1189.
[3] G.M. Staebler, Nucl. Fusion 36 (1996) 1437.
[4] N. Hayashi, et al., J. Phys. Soc. Jpn. 66 (1997) 3815.
[5] S.I. Braginskii, Reviews of Plasma Physics, vol. 1, Consultants Bureau, New York, 1966, p. 205.
[6] K. Shimizu, et al., J. Nucl. Mater. 196–198 (1992) 476.
[7] G.M. Staebler, Nucl. Fusion 31 (1991) 729.
[8] N. Hayashi, et al., Nucl. Fusion, submitted.
[9] M. Nagami, JT-60 Team, J. Nucl. Mater. 220–222 (1995) 3.
[10] K. Borrass, Nucl. Fusion 31 (1991) 1035.